JGR Atmospheres

RESEARCH ARTICLE
10.1029/2019JD030666

Revisiting Recent Elevation-Dependent Warming on the Tibetan Plateau Using Satellite-Based Data Sets

Donglin Guo[1,2], Jianqi Sun[1], Kun Yang[3], Nick Pepin[4], and Yongming Xu[5]

[1]Nansen-Zhu International Research Centre, Institute of Atmospheric Physics, Chinese Academy of Sciences, Beijing, China, [2]Key Laboratory of Meteorological Disaster, Ministry of Education/Collaborative Innovation Center on Forecast and Evaluation of Meteorological Disasters, Nanjing University of Information Science and Technology, Nanjing, China, [3]The Ministry of Education Key Laboratory for Earth System Modeling, Department of Earth System Science, Tsinghua University, Beijing, China, [4]Department of Geography, University of Portsmouth, Portsmouth, UK, [5]School of Remote Sensing and Geomatics Engineering, Nanjing University of Information Science and Technology, Nanjing, China

Key Points:

- The warming rate of satellite-based 2 m air temperatures rapidly decreases above 4,500 m despite an increase from 2,000 to 4,500 m over the Tibetan Plateau
- The decrease of warming rate above 4,500 m is conducive to less rapid decline of 83% of the current plateau solid water resources
- Changes in nighttime cloud cover and snow cover have a strong control on EDW patterns on the plateau

Correspondence to:
D. Guo,
guodl@mail.iap.ac.cn

Citation:
Guo, D., Sun, J., Yang, K., Pepin, N., & Xu, Y. (2019). Revisiting recent elevation-dependent warming on the Tibetan Plateau using satellite-based data sets. *Journal of Geophysical Research: Atmospheres*, *124*, 8511–8521. https://doi.org/10.1029/2019JD030666

Received 19 MAR 2019
Accepted 3 JUL 2019
Accepted article online 11 JUL 2019
Published online 7 AUG 2019

Abstract Satellite data, characterized by extensive regional coverage and relatively high spatial resolution, have a distinct advantage for examining elevation-dependent warming (EDW) across rugged topography in mountain regions where there are sparse in situ observations. Based on recent (2001–2015) comprehensive satellite-based data sets (2 m air temperature, land surface temperature, snow cover, and daytime and nighttime cloud), this study finds that annual mean 2 m air temperature warming rates show rapid decrease above 4,500 m despite increasing from 2,000 to 4,500 m. This indicates a reversal in EDW at the highest elevations on the Tibetan Plateau, which is somehow different from the EDW derived from short-term land surface temperature presented in earlier research. The decrease of warming rate above 4,500 m coincides with the elevation at which most of the current solid water resources reside. Thus, their decline may be less rapid than previously thought. Trends in nighttime cloud and snow cover are both correlated with patterns of EDW on the Tibetan Plateau, but the leading factor varies on an annual and seasonal basis. These results provide important evidence for understanding EDW and its controlling mechanisms in an extreme high-elevation context.

1. Introduction

In addition to the Tibetan Plateau (TP)'s vital impacts on global atmospheric circulation and climate (Wu & Chen, 1985; Yanai et al., 1992; Zhao & Chen, 2000; Zhou et al., 2009), the plateau is also the Earth's largest solid water reservoir outside the polar regions, providing life-supporting water to almost 20% of the world's population (Immerzeel et al., 2010). Areal estimates include 1.0×10^5 km^2 (glacial extent-Yao et al., 2012), 41.9×10^9 m^3/year water equivalent of snow (Li et al., 2008), and 1.1×10^6 km^2 of permafrost (Zou et al., 2017).

These reserves are vulnerable to climate warming due to their relatively warm locations in middle and low latitudes of the Northern Hemisphere (Immerzeel et al., 2010). Elevation-dependent warming (EDW), meaning systematic changes in warming rate with elevation, could pose an enhanced threat to the reservoir, mostly present at elevations above 5,000 m on the TP. Thus, understanding profiles of EDW is of great importance for future projections of water resources and associated environmental changes.

There has been a rapidly growing interest in identifying and explaining patterns of EDW on the TP (Pepin et al., 2015; Rangwala & Miller, 2012). A majority of studies indicates that warming rate is greater at higher elevations. For instance, Liu and Chen (2000) show a clear observed relationship between surface warming rate and elevation from 1960 to 1990. Similar results are produced using the Goddard Institute for Space Studies-Atmosphere Ocean Model global climate model for both historical and future periods (Rangwala et al., 2010). Nevertheless, other studies indicate no significant relationship between warming rate and elevation. An example is the analysis of You et al. (2010) based on observations and reanalysis data for 1961–2005. The divergence in results may be due to differences in the number of stations compared, the temporal and spatial resolutions of the data (e.g., annual vs. seasonal and tmin/tmax vs. mean temperature), and the time periods chosen (Pepin et al., 2015). Given that mountain regions are topographically complex and demonstrate distinct microclimates, rigorous identification of EDW ideally requires both high spatial

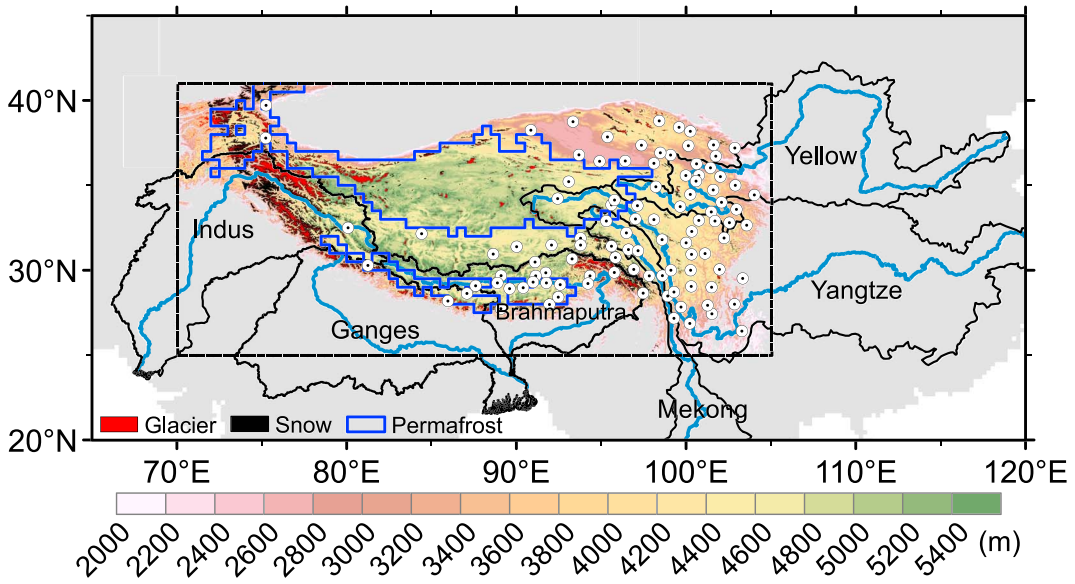

Figure 1. Location of the study region (the Tibetan Plateau; areas with elevation >2,000 m within the block 70–105°E, 25–41°N); the location of current solid water resources (glacial extent, snow, and permafrost); related basins and river courses in Southeast Asia; and China Meteorological Administration weather stations (white dots).

resolution and extensive spatial extent. Unfortunately, weather stations are extremely sparse on the TP, particularly in western regions. Despite adequate spatial coverage, reanalysis data sets and models have relatively poor spatial resolution and require sufficient numbers of in situ observations for validation (Wang & Zeng, 2012).

Satellite monitoring in theory allows studies to overcome the spatial resolution and areal extent inadequacies inherent in point observations, gridded reanalyses, and models, and they have been suggested to be a future research focus by the Mountain Research Initiative EDW Working Group (Pepin et al., 2015). Qin et al. (2009) investigated EDW on the TP as a whole using nighttime MODIS land surface temperatures (LST) between 2000 and 2006. However, the data employed in Qin et al. (2009) cover only 7 years, too short to detect warming trends (Yang et al., 2014). Qin et al. (2009) used LST, which differs substantially from 2 m air temperature, particularly at high elevations, due to vegetation and snow cover effects (Pepin et al., 2016). 2 m air temperature (screen level 2 m above ground level) is the agreed essential climate variable used to identify both EDW and regional patterns of climate change (IPCC, 2013), so some attempt must be made to correct LST to more closely represent 2 m air temperature if it is to be of wide application for climate change research.

The aim of this study is to use recent (2001–2015) comprehensive satellite-based data sets to identify patterns in EDW and their driving factors on the TP as a whole, at a 1-km resolution. The data sets used include satellite-based 2 m air temperature (SBAT), Moderate Resolution Imaging Spectroradiometer (MODIS)-based LST, snow cover, and daytime/nighttime cloud extent. Comparing spatial patterns in various factors will advance our understanding of both the patterns in EDW observed and of the associated mechanisms that are responsible for these patterns on the TP.

2. Data and Methods

Although LST can be directly derived from MODIS data, 2 m air temperatures are commonly used for research on EDW rather than LST. Thus, we used a satellite-based 2 m air temperature (SBAT) data set developed using machine learning models based on MODIS LST combined with normalized difference vegetation index data, Shuttle Radar Topography Mission digital elevation model data, solar radiation, and topographic index data. For details see Xu et al. (2018). The data are available at the Shallow Water Earth Observation Lab website (https://www.shallowwaterlab.com/single-post/2018/01/25/

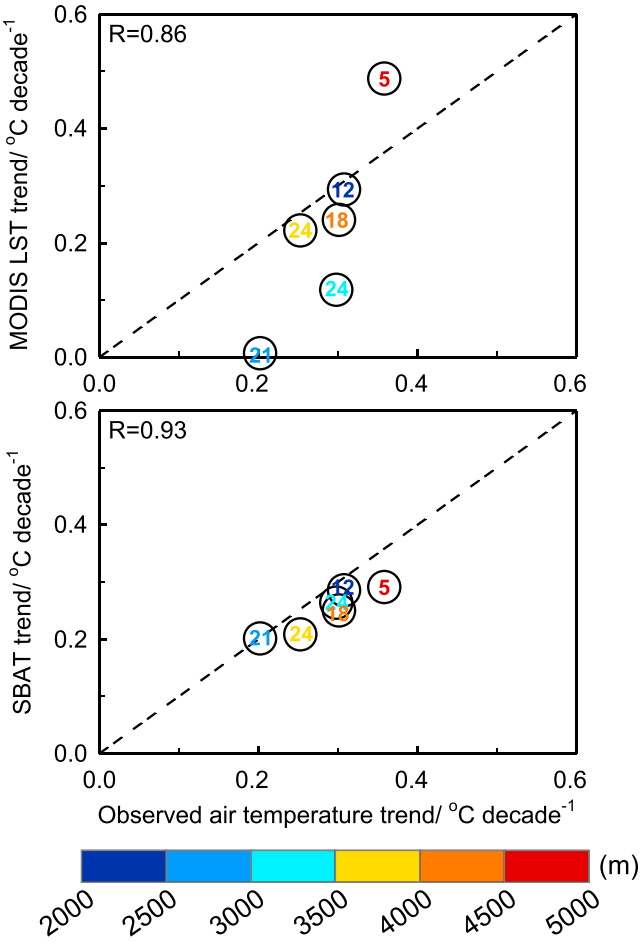

Figure 2. Comparison between trends in (a) annual mean Moderate Resolution Imaging Spectroradiometer (MODIS) land surface temperature (LST) and (b) satellite-based 2 m air temperature (SBAT) and the pixel-corresponding weather station trends for individual elevation bins for 2001 to 2015. The number in each circle in both panels represents the number of weather stations in each elevation bin. The color of the number in each circle in panels (a) and (b) corresponds to the elevation bin represented by the color bar. *R* is the correlation coefficient between MODIS LST/SBAT and weather station temperature trends.

Tracking-temperature-in-Tibet). Compared with observed EDW from in situ weather stations (Figure 1), SBAT shows better correspondence (correlation coefficient [r] = 0.93) than MODIS LST (r = 0.86; Figure 2). Moreover, the former is distinctly closer to the 1:1 line in the scatterplot. Comparison using individual station/pixel trends (rather than elevation-bin means) also shows SBAT to more closely approximate air temperature than MODIS LST (Figure 3). Thus, SBAT is used to identify EDW in the present study rather than MODIS LST. This data set has a resolution of 1 km across the entire TP and covers the period 2001–2015.

The MODIS normalized difference snow index (NDSI) and cloud amount are used to represent possible driving factors of EDW. NDSI is calculated as the difference between observed reflectance in visible and shortwave infrared bands. Hall et al. (1995) and Tang et al. (2013) show that MODIS NDSI can effectively discriminate snow from other surface cover types. Thus, we used the daily MODIS NDSI product (MOD10A1, v6) to represent snow cover in this study. The mean monthly frequencies of cloud cover (calculated as cloud days/total days in a month) for daytime (local time ~10:30) and nighttime (local time ~22:30) are calculated from the MODIS cloud mask product (MOD35; Ackerman et al., 2010). Both snow cover and cloud frequency data sets cover the period 2001–2015 and have a common resolution of 1 km.

2 m air temperatures recorded at 104 China Meteorological Administration weather stations (2001–2015) are used to validate SBAT. Observations are mostly concentrated in the central/eastern TP, with only 12 stations in the western region, west of 90°E (Figure 1). Quality control of the station data, based on logical testing and comparison with surrounding stations, is described in Li et al. (2004). These data have been widely used in previous research on climate change (Gou &Wang 2012; Guo et al., 2018).

Data on glacier, permafrost, and snow cover extent were used to illustrate the impact of variable warming rates on solid water reserves. The glacial extent comes from the Global Land Ice Measurements from Space data set (GLIMS and NSIDC, 2017), derived from the National Snow and Ice Data Center (http://glims.colorado.edu/glacierdata/). The format consists of Environmental Systems Research Institute shape files. Permafrost extent was obtained from the Arctic map of permafrost and ground ice conditions (Brown et al., 1997), which quantifies the extent of continuous, discontinuous, isolated, and sporadic permafrost. Only continuous and discontinuous permafrost are classed as containing solid water resources. The data are archived at the website (http://nsidc.org/data/) at a resolution of 0.5° × 0.5°. The extent of the snow-covered area is defined as that having over 6 months' snow coverage in an average year (2004–2010). Snow cover data come from the MODIS daily snow product after cloud removal (Huang et al., 2012), obtained from the Environmental and Ecological Science Data Center for West China, National Natural Science Foundation of China (http://westdc.westgis.ac.cn). Glacial extent, permafrost, and snow cover extent were resampled (aggregated) to a common resolution of 1 km for comparison. Nearest neighbor interpolation was used to ensure that the spatial extents of each parameter were consistent before and after resampling. Their spatial distributions can be seen in Figure 1.

Surface elevation was quantified using global digital elevation data (GTOPO30), derived from the U.S. Geological Survey's Center for Earth Resources Observation and Science (1-km resolution). Linear trends of temperature, snow cover, and cloud amount are calculated using the slope of the ordinary least squares regression line, and their statistical significances are evaluated using the Student's t test.

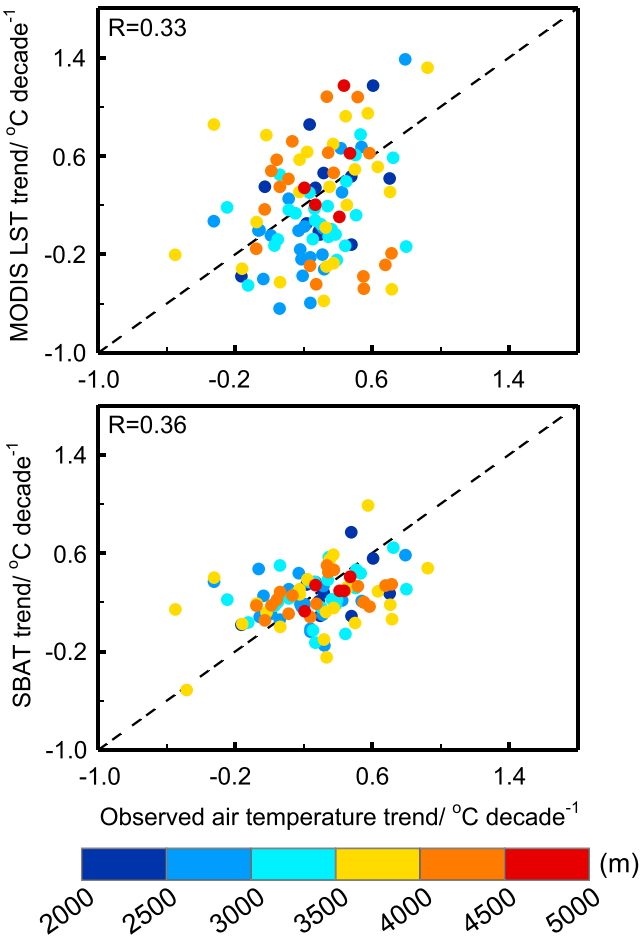

Figure 3. Comparison between (a) annual Moderate Resolution Imaging Spectroradiometer (MODIS) land surface temperature (LST) and (b) satellite-based 2 m air temperature (SBAT) trends and the pixel-corresponding weather station trends for 104 individual stations/pixels for 2001 to 2015. The colors of circles in panels (a) and (b) correspond to the elevation bin represented by the color bar. *R* is the correlation coefficient between MODIS LST or SBAT and weather station air temperature trends.

3. Results

3.1. Patterns of EDW on the TP

Warming rates for annual SBAT (2001–2015) increase with elevation from 2,000 to 4,500 m but rapidly decrease above this elevation (Figure 4). This suggests a reversal in EDW above 4,500 m in recent years. SBAT trends are similar to those based on station observations between 2,000 and 4,500 m. However, the station-based trends continue to increase up to 5,000 m, whereas SBAT trends decrease. Because there are only five stations above 4,500 m, the station trend is somewhat uncertain. Past research has shown that multiple stations (>10) are required to eliminate spatial differences between MODIS LST and station-observed trends (Qin et al., 2009). Elevational profiles of seasonal SBAT warming rates are broadly similar in form to the annual profile except the elevations at which peak warming occurs are different (spring, 4,000–4,500 m; summer, 3,500–4,000 m; autumn, 6,000–6,500 m; and winter, 3,500–4,000 m; Figure 5). The season with higher elevation of peak warming has larger warming rate, consistent with the findings from Guo et al. (2016).

A majority (glacier, 89%; snow, 83%; and permafrost, 77%, as identified by area) of the solid water resources of the TP is located above 4,500 m (Figure 4). The decrease of SBAT warming rate at 4,500 m and above could be relatively beneficial for this solid water resource, meaning that it may not ablate as fast as previously envisaged. To examine this in more detail, we calculate elevation gradients in SBAT trends over glacier, snow, and permafrost regions alone (Figure 6). For glacier and snow regions, SBAT trends indeed decrease with increasing elevation. For permafrost regions, SBAT trends behave in a similar way to those based on the entire TP (unsurprising due to the larger spatial extent). Although SBAT trends decrease with increasing elevation, they are still positive, so the decrease in trend magnitude will not prevent the long-term loss of the solid water resources, even if they encourage a less rapid decline.

3.2. Driving Mechanisms of EDW Patterns: Correlation of Warming Trends With Other Variables

To interpret the physical causes of the EDW patterns observed, we examine the correlation between SBAT trends and simultaneous trends in snow cover and day/night cloud amount. Annual and seasonal relationships between SBAT trends and trends in cloud and snow for 12 elevation bins are shown in Figure 7. On an annual basis, nighttime cloud trends are statistically significantly correlated with SBAT trends ($r = 0.68$, $p < 0.02$). Thus, increasing nighttime cloud encourages faster warming rates by enhancing atmospheric counter-radiation (downward longwave radiation) and subsequently weakening effective terrestrial radiation (Rangwala & Miller, 2012). There is also a positive correlation between trends in daytime cloud cover and SBAT trends on an annual basis.

Annual snow cover trends also have a significant correlation with SBAT trends below 5,000 m ($r = -0.87$, $p < 0.05$) but show no close relationship above 5,000 m (Figure 8). As expected, reduction in snow cover is correlated with stronger warming.

On a seasonal basis, snow cover is statistically significantly correlated with SBAT trends in spring ($r = -0.60$, $p < 0.05$) and winter ($r = -0.66$, $p < 0.02$; Figures 7 and 8), when snow cover is typically extensive. Nighttime cloud is a strong control in spring ($r = 0.83$, $p < 0.01$) and autumn ($r = 0.61$, $p < 0.05$). In the latter season (when snow is limited below 6,000 m), nighttime cloud appears to be the leading driving factor. All three variables show no significant correlation with SBAT trends in summer, meaning that further work needs to understand the factors in this season. The different driving factors of SBAT trends in different seasons

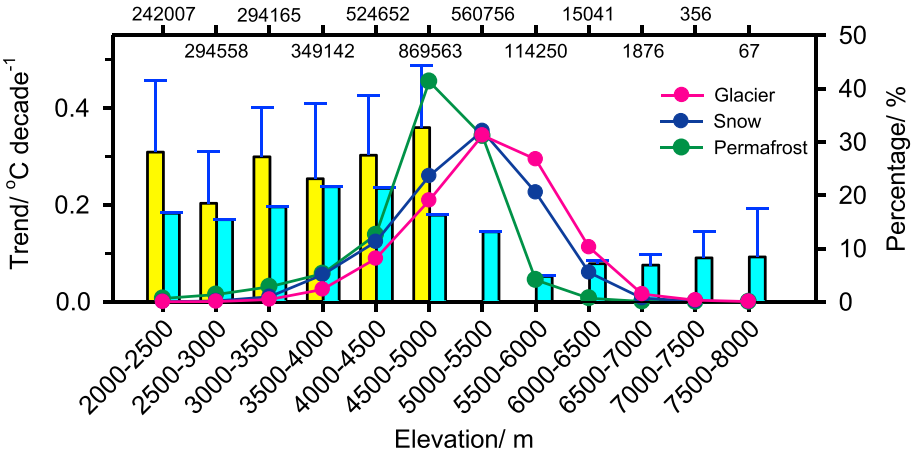

Figure 4. Change of annual mean weather station 2 m air temperature (yellow bar) and satellite-based 2 m air temperature (cyan bar) trends for 2001 to 2015 compared with the elevation distribution of solid water resources (glacial extent, snow, and permafrost areas). Trends are mean values over individual elevation bins. Percentages (right axis) are calculated as (water resource area in individual elevation bin)/(water resource area over the whole Tibetan Plateau: 2,000–8,000 m) × 100%. The number on the top of the figure is the number of satellite pixels in the corresponding elevation bin. Blue error bars are based on 95% confidence intervals around the mean.

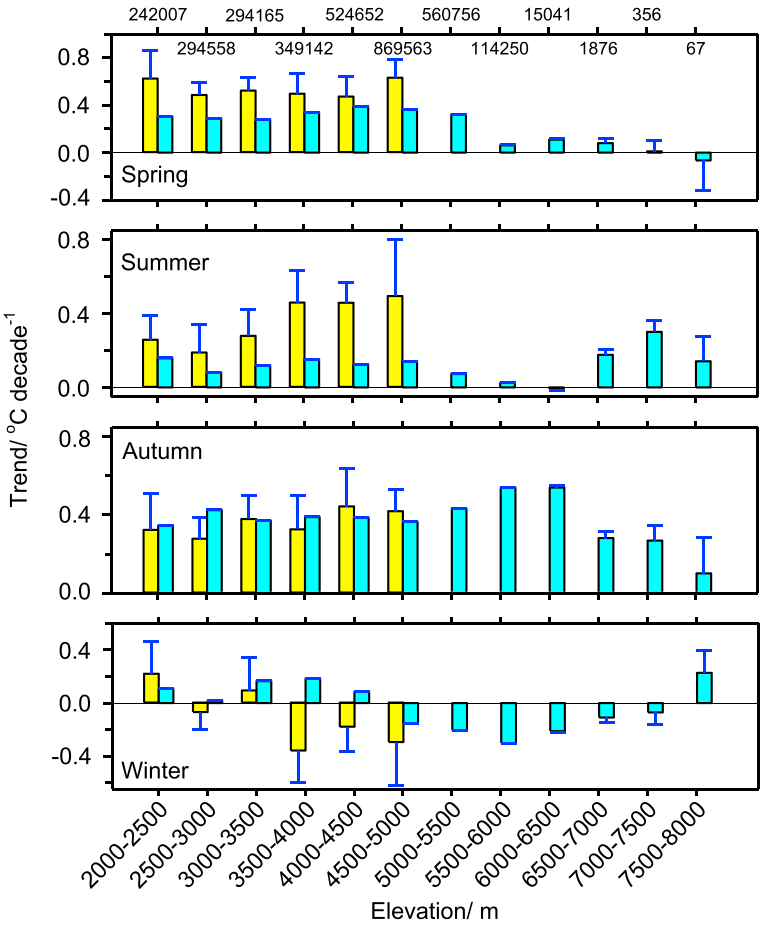

Figure 5. Seasonal patterns of mean weather station 2 m air temperature (yellow bar) and satellite-based 2 m air temperature (cyan bar) trends for 2001 to 2015. Trends are mean values over individual elevation bins. The numbers on the top of the spring panel are the number of satellite pixels in the corresponding elevation bin. Blue error bars are based on 95% confidence intervals around the mean.

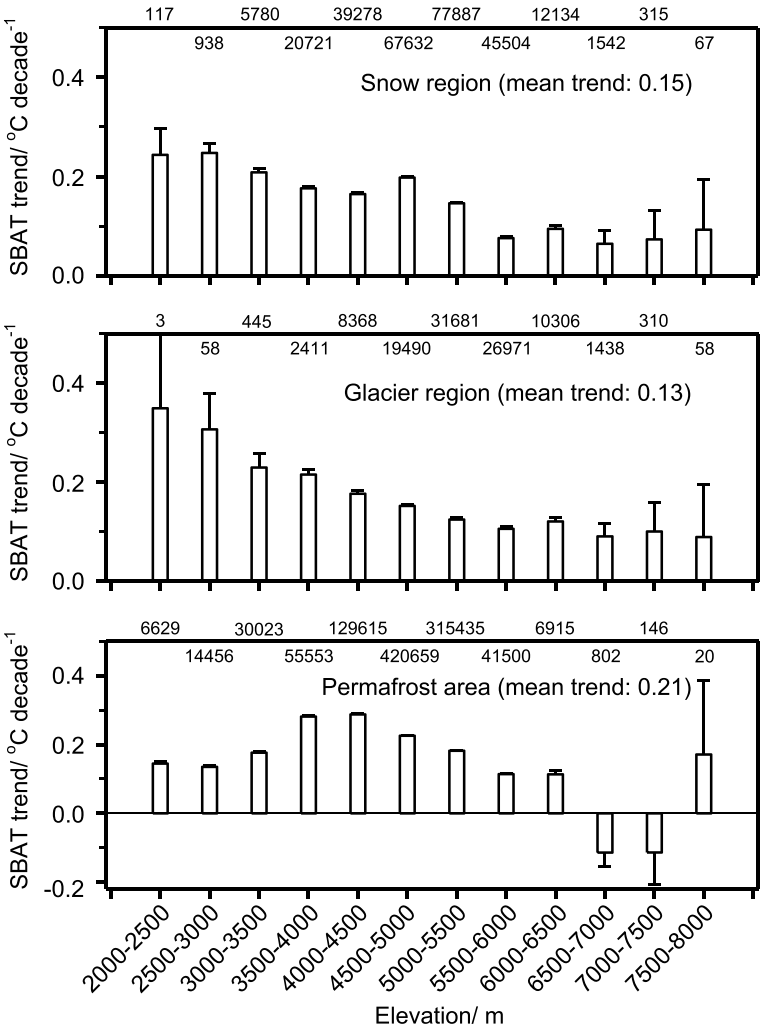

Figure 6. Annual mean satellite-based 2 m air temperature (SBAT) trends (2001–2015) for individual elevation bins concentrated over snow, glacier, and permafrost regions on the Tibetan Plateau. The numbers on the top of the panels are the numbers of satellite pixels in the corresponding elevation bin. Error bars are based on 95% confidence intervals around the mean.

are perhaps unsurprising given the strong monsoonal regime and variable snowline elevation throughout the year.

4. Discussions

4.1. Comparison With Previous Studies on EDW

Based on nighttime MODIS LST between 2000 and 2006, Qin et al. (2009) showed an increasing warming rate with elevation from 3,000 up to 4,800 m, similar to our results. Our study finds a rapid decrease in warming rate from 4,500 to 6,500 m; in contrast, they showed a more stable warming rate as elevation increases from about 4,800 to 6,400 m. Their differences may be due to two causes. First, data employed in Qin et al. (2009) covered a 7-year period, which is much shorter than the one used in this study. Second, the LST used by Qin et al. (2009) differs substantially from SBAT used in this study because of strong vegetation and snow effects on LST at high elevations (Pepin et al., 2016). We calculated the EDW from MODIS LST and SBAT (Figure 9). The result shows that elevational profile of warming rate of MODIS LST is similar to that of SBAT from 2001 to 2015 but warming rates start to decrease above 5,500 m rather than 4,500 m (SBAT). This indicates that the EDW difference between this study and Qin et al. (2009) is affected by both the study

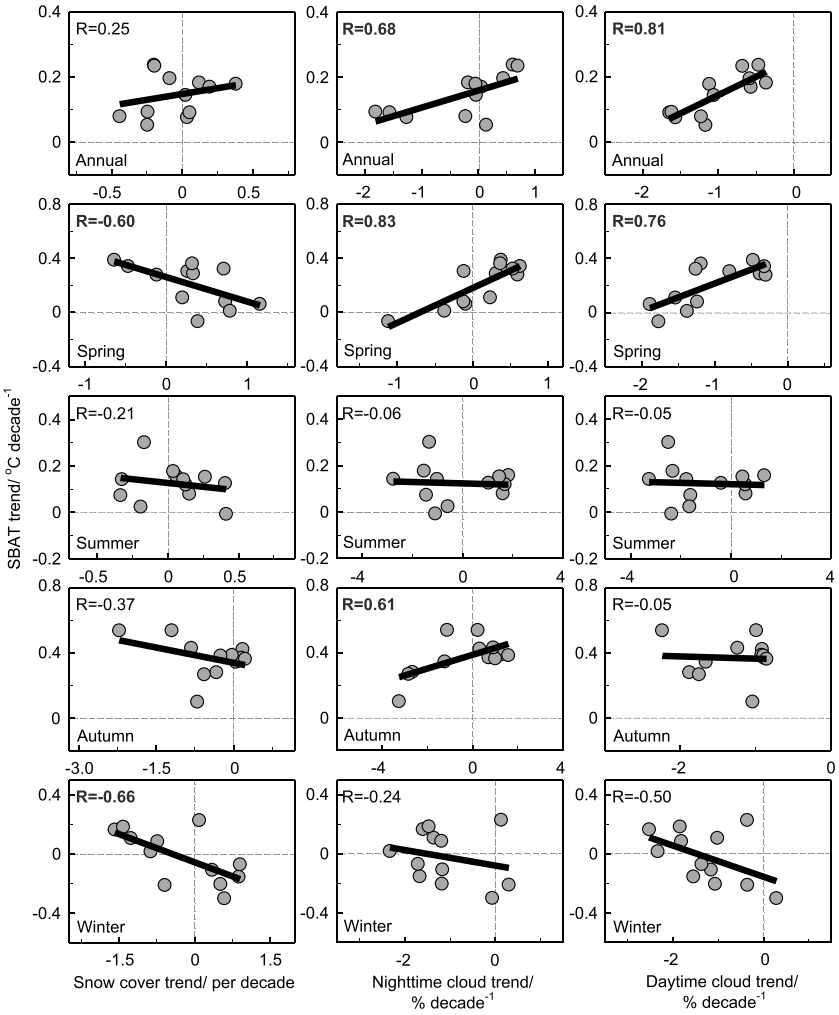

Figure 7. Correlations between mean satellite-based 2 m air temperature (SBAT) trends (2001–2015) and simultaneous snow cover trends (left), nighttime cloud trends (middle), and daytime cloud trends (right) for 12 elevation bins (shown in Figure 4). Rows refer to the annual mean trend (top row) followed by spring, summer, autumn, and winter. Solid lines represent regression lines. *R* is the correlation coefficient between SBAT trends and the corresponding variable trends (significant at $p < 0.05$ if in bold).

periods and the variables used for calculating warming rates. Furthermore, our results are supported by model simulations that show a reduction in warming rate above about 5,000 m on the TP during the present day and near future (Gao et al., 2018; Guo et al., 2016).

4.2. Discussions on Driving Mechanisms of EDW

Previous studies have attributed EDW patterns to changes in snow-albedo feedback (Guo et al., 2016; Rangwala et al., 2010; Yan et al., 2016), cloud-radiation effects (Liu et al., 2009), the downwelling effect of water vapor on longwave radiation (Palazzi et al., 2017; Rangwala et al., 2010), and aerosols (Xu et al., 2016). Our analysis of controlling factors (Figure 7) throws light on the relative importance of possible mechanisms that could control EDW in the TP. Decline of snow cover is strongly correlated with temperature trends in winter and spring, and the peak SBAT warming at 3,500–4,000 and 4,000–4,500 m in the two seasons, respectively, is strong evidence of snow-albedo feedback enhancing warming in these elevation bands. Changes in cloud amounts are also often important. Cloud cover is a proxy for atmospheric moisture content. Increases in cloud cover enhances warming rates through enhanced downwelling of longwave radiation due to increased water vapor (Rangwala & Miller, 2012). Due to the nonlinear relationship between specific humidity and downwelling of longwave radiation, this is particularly important in spring

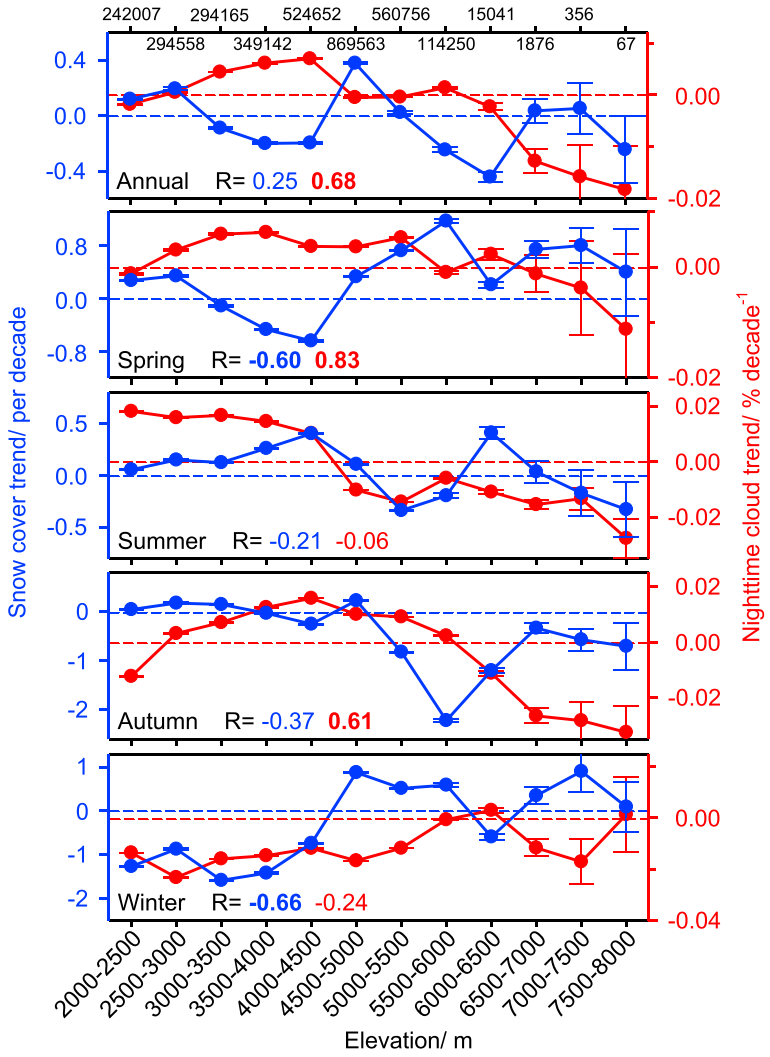

Figure 8. Elevational profiles of trends in annual and seasonal mean snow cover (blue) and nighttime cloud amount (red) for 2001 to 2015. Trends are mean values over individual elevation bins. The numbers on the top of the annual panel are the numbers of satellite pixels in the corresponding elevation bin. *R* is the correlation coefficient between snow cover or nighttime cloud trends and corresponding satellite-based 2 m air temperature trends. Bold figures represent correlations significant at $p < 0.05$.

and autumn at night when current water vapor levels are low. Perhaps surprisingly, increased daytime cloud cover is also a control of SBAT trends on an annual basis, again with more cloud leading to more warming. The consistency of the cloud effect between day and night suggests that it is attendant reductions in free-air lapse rates (tending to a saturated adiabatic lapse rate profile rather than dry adiabatic lapse rate) and the increased downwelling effect, rather than the direct effect of clouds on surface temperatures (which reverses from day to night), which is driving the EDW response in this case. More moist cloudy conditions lead to a shallower atmospheric lapse rate, preferentially warming high elevations. At extremely high elevations (>5,000 m), cloudy days can often be warmer than clear ones, especially in low latitudes where the difference between saturated adiabatic lapse rate and dry adiabatic lapse rate can be large.

Many previous studies have employed model simulations to investigate similar forcing mechanisms. There are two serious limitations; (i) many models show poor performance on the TP (Guo et al., 2016; Su et al., 2013) due to the complex terrain, which may have large impacts on our mechanistic understanding of EDW; (ii) the model-based relationships between driving factors and EDW may be intrinsic to physical

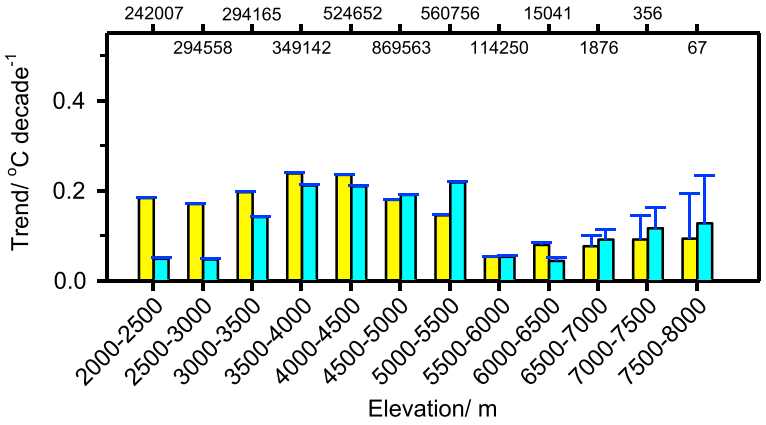

Figure 9. Change of annual mean satellite-based 2 m air temperature (yellow bar) and Moderate Resolution Imaging Spectroradiometer land surface temperature (cyan bar) trends for 2001 to 2015. Trends are mean values over individual elevation bins. The numbers on the top of the figure are the numbers of satellite pixels in the corresponding elevation bin. Blue error bars are based on 95% confidence intervals around the mean.

schemes used and thus need validation from observations. Weather station observations have also been used to explore mechanisms, but they are restricted to valley locations in the central and eastern TP (Duan & Wu, 2006; Rangwala et al., 2009), so provide an incomplete picture. Based on comprehensive satellite-based data sets, this study indicates that overall, both cloud and snow cover are leading driving factors for EDW though they function differently on an annual basis and during the four seasons. Our study provides important satellite-based evidence for understanding the controlling mechanisms of EDW and can be considered as a strong validation of previous research using model simulations.

4.3. Discussion on the Impacts of EDW on Water Resources

Glaciers, snow, and permafrost are concentrated in the critical elevation zone above 4,500 m, so the rate of warming above this elevation is a strong determinant of the rate of future decline of these resources. Temperature trends in SBAT are still positive, so the reduction in rate of warming above 4,500 m may lead to a less rapid decline in water resources than thought, but not necessarily their preservation in the long term. Caution is also needed in extrapolating patterns in recent change to the near future, because as the snowline retreats upslope in future, peak spring warming rate may move uphill from 4,500 m as forcing factors also change. Thus, the elevational profile of recent trends may not necessarily represent the future profile, EDW being a dynamic phenomenon (Guo et al., 2016; Pepin et al., 2015). The warming rate is already high (~0.23 °C/decade) at 4,000–4,500 m, and this high rate could extend to higher elevations.

4.4. Analysis of Potential Uncertainties

Potential uncertainties may be related to the datasets used. SBAT is the most important dataset in this study. It has an overall root mean square error (RMSE) of 1.0 °C, and mean absolute error (MAE) of 0.73 °C according to tenfold cross-validation against station air temperature on an annual basis (Xu et al., 2018). When SBAT is compared to two reanalysis data sets (National Centers for Environmental Prediction-Reanalysis 2 and European Centre for Medium-Range Weather Forecasts Reanalysis Interim), it shows distinctly better performance: National Centers for Environmental Prediction-Reanalysis 2 has a RMSE of 8.62 °C and MAE of 7.58 °C, and European Centre for Medium-Range Weather Forecasts Reanalysis Interim has a RMSE of 5.55 °C and MAE of 4.6 °C. Validations in this study show that SBAT reasonably reproduces the EDW profile from station data. The correlation coefficient between trends is 0.93 and exceeds the 99% significance level. This indicates that errors in SBAT contribute only a small uncertainty to the research results.

The MODIS LST product (MOD11A1, V6) is also used to compare to SBAT in this study. Several studies have validated that this product has reasonable accuracy (errors less than 1 °C for most cases; Wan, 2014; Duan et al., 2018). The MODIS cloud mask product shows good agreement with the Cloud-Aerosol Lidar with Orthogonal Polarization cloud product, with global consistency ranging from 77.8% to 87.1% (Ackerman et al., 2010; Wang et al., 2016). It should be mentioned that the above biases in these products are often

largely systematic—a type of bias that deviates by a fixed amount from the true value. This study only uses linear trends calculated from these products. Systematic biases are removed when calculating the trends. In other words, final uncertainty in the trend analysis is often smaller than original biases because of the removal of the systematic component. In spite of this, biases in these products may still contribute to at least part of the uncertainties in the research results.

Because of the limitation of the period of satellite data, our study investigates EDW during very recent decades. Such a period may not indicate long-term tendencies of climate change on the TP. However, as satellite data lengthens, we will be able to analyze trends over the extended observation periods.

5. Conclusion

Using comprehensive satellite-based data sets, we examined EDW and its driving factors over the entire TP from 2001 to 2015. The satellite-based warming rate shows an increasing magnitude from 2,000 to 4,500 m but rapidly decreases above this (4,500–6,000 m). The decrease in rate of warming above 4,500 m is conducive to the maintenance (or at least less rapid decline) of most (83% by area) of the solid water resources across the TP. Changes in nighttime cloud and snow cover appear to be the dominant controls of observed EDW, but the most important factor differs for mean annual temperatures and in different seasons. These results are useful for assessing the sustainability of water resources in the context of recently rapidly changing climate on the TP.

Acknowledgments
This research was jointly supported by the National Key R&D Program of China (2016YFA0600704), the National Natural Science Foundation of China (41775076), and Youth Innovation Promotion Association CAS. We thank the National Snow and Ice Data Center (Boulder, CO, USA) for providing the Circum-Arctic Map of Permafrost and Ground-Ice Conditions (http://nsidc.org/data/) and the glacial extent data (http://glims.colorado.edu/glacierdata/). We are indebted to Professor Xiaodong Liu from the Institute of Earth Environment, Chinese Academy of Sciences, for his constructive comments and discussions during preparation of this study.

References

Ackerman, S., Frey, R., Strabala, K., Liu, Y., Gumley, L., Baum, B., & Menzel, P. (2010). Discriminating clear-sky from cloud with MODIS algorithm theoretical basis document (MOD35). Cooperative Institute for Meteorological Satellite Studies, University of Wisconsin-Madison.

Brown, J., Ferrians, J., Heginbottom, J., & Melnikov, E. (1997). Circum-Arctic map of permafrost and ground-ice conditions. US Geological Survey in Cooperation with the Circum-Pacific Council for Energy and Mineral Resources, Circum-Pacific Map Series CP-45, scale 1:10,000,000, 1 sheet.

Duan, A., & Wu, G. (2006). Change of cloud amount and the climate warming on the Tibetan Plateau. *Geophysical Research Letters*, *33*, L22704. https://doi.org/10.1029/2006GL027946

Duan, S., Li, Z., Wu, H., Leng, P., Gao, M., & Wang, C. (2018). Radiance-based validation of land surface temperature products derived from Collection 6 MODIS thermal infrared data. *International Journal of Applied Earth Observation and Geoinformation*, *70*, 84–92. https://doi.org/10.1016/j.jag.2018.04.006

Gao, Y., Chen, F., Lettenmaier, D., Xu, J., Xiao, L., & Li, X. (2018). Does elevation-dependent warming hold true above 5000 m elevation? Lessons from the Tibetan Plateau. *npj Climate and Atmospheric Science*, *1*(1). https://doi.org/10.1038/s41612-018-0030-z

GLIMS & NSIDC. (2017). Global land ice measurements from space glacier database. Compiled and made available by the international GLIMS community and the National Snow and Ice Data Center, Boulder CO, U.S.A.

Guo, D., Sun, J., & Yu, E. (2018). Evaluation of CORDEX regional climate models in simulating temperature and precipitation on the Tibetan Plateau. *Atmospheric and Oceanic Science Letters*, *11*(3), 219–227. https://doi.org/10.1080/16742834.2018.1451725

Guo, D., & Wang, H. (2012). The significant climate warming in the northern Tibetan Plateau and its possible causes. *International Journal of Climatology*, *32*(12), 1775–1781. https://doi.org/10.1002/joc.2388

Guo, D., Yu, E., & Wang, H. (2016). Will the Tibetan Plateau warming depend on elevation in the future? *Journal of Geophysical Research: Atmospheres*, *121*, 3969–3978. https://doi.org/10.1002/2016JD024871

Hall, D., Riggs, G., & Salomonson, V. (1995). Development of methods for mapping global snow cover using Moderate Resolution Imaging Spectroradiometer data. *Remote Sensing of Environment*, *54*(2), 127–140. https://doi.org/10.1016/0034-4257(95)00137-P

Huang, X., Hao, X., Wang, W., Feng, Q., & Liang, T. (2012). Algorithms for cloud removal in MODIS daily snow products. *Journal of Glaciology and Geocryology*, *34*, 1118–1126.

Immerzeel, W., Van Beek, L., & Bierkens, M. (2010). Climate change will affect the Asian water towers. *Science*, *328*(5984), 1382–1385. https://doi.org/10.1126/science.1183188

IPCC (2013). Summary for policymakers. In T. F. Stocker, et al. (Eds.), *Climate change 2013: The physical science basis. Contribution of Working Group I to the Fifth Assessment Report of the Intergovernmental Panel on Climate Change*, (pp. 3–29). Cambridge, U. K.: Cambridge Univ. Press.

Li, Q., Liu, X., Zhang, H., Peterson, T., & Easterling, D. (2004). Detecting and adjusting on the temporal inhomogeneity in Chinese mean surface air temperature dataset. *Advances in Atmospheric Sciences*, *21*(2), 260–268. https://doi.org/10.1007/BF02915712

Li, X., Cheng, G., Jin, H., Kang, E., Che, T., Jin, R., et al. (2008). Cryospheric change in China. *Global and Planetary Change*, *62*(3-4), 210–218. https://doi.org/10.1016/j.gloplacha.2008.02.001

Liu, X., & Chen, B. (2000). Climatic warming in the Tibetan Plateau during recent decades. *International Journal of Climatology*, *20*(14), 1729–1742. https://doi.org/10.1002/1097-0088(20001130)20:14<1729::AID-JOC556>3.0.CO;2-Y

Liu, X., Cheng, Z., Yan, L., & Yin, Z. (2009). Elevation dependency of recent and future minimum surface air temperature trends in the Tibetan Plateau and its surroundings. *Global and Planetary Change*, *68*(3), 164–174. https://doi.org/10.1016/j.gloplacha.2009.03.017

Palazzi, E., Mortarini, L., Terzago, S., & Hardenberg, J. (2017). Elevation-dependent warming in global climate model simulations at high spatial resolution. *Climate Dynamics*, *52*, 2685–2702.

Pepin, N. C., Bradley, R. S., Diaz, H., Baraer, M., Caceres, E., Forsythe, N., et al. (2015). Elevation-dependent warming in mountain regions of the world. *Nature Climate Change*, *5*, 424–430.

Pepin, N. C., Maeda, E. E., & Williams, R. (2016). Use of remotely sensed land surface temperature as a proxy for air temperatures at high elevations: Findings from a 5000 m elevational transect across Kilimanjaro. *Journal of Geophysical Research: Atmospheres*, *121*, 9998–10,015. https://doi.org/10.1002/2016JD025497

Qin, J., Yang, K., Liang, S., & Guo, X. (2009). The altitudinal dependence of recent rapid warming over the Tibetan Plateau. *Climatic Change*, *97*(1-2), 321–327. https://doi.org/10.1007/s10584-009-9733-9

Rangwala, I., & Miller, J. (2012). Climate change in mountains: a review of elevation-dependent warming and its possible causes. *Climatic Change*, *114*(3-4), 527–547. https://doi.org/10.1007/s10584-012-0419-3

Rangwala, I., Miller, J., Russell, G., & Xu, M. (2010). Using a global climate model to evaluate the influences of water vapor, snow cover and atmospheric aerosol on warming in the Tibetan Plateau during the twenty-first century. *Climate Dynamics*, *34*(6), 859–872. https://doi.org/10.1007/s00382-009-0564-1

Rangwala, I., Miller, J., & Xu, M. (2009). Warming in the Tibetan Plateau: Possible influences of the changes in surface water vapor. *Geophysical Research Letters*, *36*, L06703. https://doi.org/10.1029/2009GL037245

Su, F., Duan, X., Chen, D., Hao, Z., & Cuo, L. (2013). Evaluation of the global climate models in the CMIP5 over the Tibetan Plateau. *Journal of Climate*, *26*(10), 3187–3208. https://doi.org/10.1175/JCLI-D-12-00321.1

Tang, B., Shrestha, B., Li, Z., Liu, G., Ouyang, H., Gurung, D., et al. (2013). Determination of snow cover from MODIS data for the Tibetan Plateau region. *International Journal of Applied Earth Observation and Geoinformation*, *21*, 356–365. https://doi.org/10.1016/j.jag.2012.07.014

Wan, Z. (2014). New refinements and validation of the collection-6 MODIS land-surface temperature/emissivity product. *Remote Sensing of Environment*, *140*, 36–45. https://doi.org/10.1016/j.rse.2013.08.027

Wang, A., & Zeng, X. (2012). Evaluation of multireanalysis products with in situ observations over the Tibetan Plateau. *Journal of Geophysical Research*, *117*, D05102. https://doi.org/10.1029/2011JD016553

Wang, T., Fetzer, E., Wong, S., Kahn, B., & Yue, Q. (2016). Validation of MODIS cloud mask and multilayer flag using CloudSat-CALIPSO cloud profiles and a cross-reference of their cloud classifications. *Journal of Geophysical Research: Atmospheres*, *121*, 620–635. https://doi.org/10.1002/2016JD025239

Wu, G., & Chen, S. (1985). The effect of mechanical forcing on the formation of a mesoscale vortex. *Quarterly Journal of the Royal Meteorological Society*, *21*, 1049–1070.

Xu, Y., Knudby, A., Shen, Y., & Liu, Y. (2018). Mapping monthly air temperature in the Tibetan Plateau from MODIS data based on machine learning methods. *IEEE Journal of Selected Topics in Applied Earth Observations and Remote Sensing*, *11*(2), 345–354. https://doi.org/10.1109/JSTARS.2017.2787191

Xu, Y., Ramanathan, V., & Washington, W. (2016). Observed high-altitude warming and snow cover retreat over Tibet and the Himalayas enhanced by black carbon aerosols. *Atmospheric Chemistry and Physics*, *16*(3), 1303–1315. https://doi.org/10.5194/acp-16-1303-2016

Yan, L., Liu, Z., Chen, G., Kutzbach, J., & Liu, X. (2016). Mechanisms of elevation-dependent warming over the Tibetan plateau in quadrupled CO_2 experiments. *Climatic Change*, *135*(3-4), 509–519. https://doi.org/10.1007/s10584-016-1599-z

Yanai, M., Li, C., & Song, Z. (1992). Seasonal heating of the Tibetan Plateau and its effects on the evolution of the Asian summer monsoon. *Journal of the Meteorological Society of Japan*, *70*(1B), 319–351. https://doi.org/10.2151/jmsj1965.70.1B_319

Yang, K., Wu, H., Qin, J., Lin, C., Tang, W., & Chen, Y. (2014). Recent climate changes over the Tibetan Plateau and their impacts on energy and water cycle: A review. *Global and Planetary Change*, *112*, 79–91. https://doi.org/10.1016/j.gloplacha.2013.12.001

Yao, T. D., Thompson, L., Mosbrugger, V., Zhang, F., Ma, Y., Luo, T., et al. (2012). Third pole environment (TPE). *Environmental Development*, *3*, 52–64. https://doi.org/10.1016/j.envdev.2012.04.002

You, Q., Kang, S., Pepin, N., Flügel, W., Yan, Y., Behrawan, H., & Huang, J. (2010). Relationship between temperature trend magnitude, elevation and mean temperature in the Tibetan Plateau from homogenized surface stations and reanalysis data. *Global and Planetary Change*, *71*(1-2), 124–133. https://doi.org/10.1016/j.gloplacha.2010.01.020

Zhao, P., & Chen, L. (2000). Study on climatic features of surface turbulent heat exchange coefficients and surface thermal sources over the Qinghai–Xizang (Tibetan) Plateau. *Acta Meteorologica Sinica*, *14*, 13–29.

Zhou, X., Zhao, P., Chen, J., Chen, L., & Li, W. (2009). Impacts of thermodynamic processes over the Tibetan Plateau on the Northern Hemispheric climate. *Science China Earth Sciences*, *52*(11), 1679–1693. https://doi.org/10.1007/s11430-009-0194-9

Zou, D., Zhao, L., Sheng, Y., Chen, J., Hu, G., Wu, T., et al. (2017). A new map of permafrost distribution on the Tibetan Plateau. *The Cryosphere*, *11*(6), 2527–2542. https://doi.org/10.5194/tc-11-2527-2017